A Four-Step Mechanism for the Formation of Supported-Nanoparticle Heterogenous Catalysts in Contact with Solution: The Conversion of Ir(1,5-COD)Cl/γ-Al$_2$O$_3$ to Ir(0)$_{\sim170}$/γ-Al$_2$O$_3$
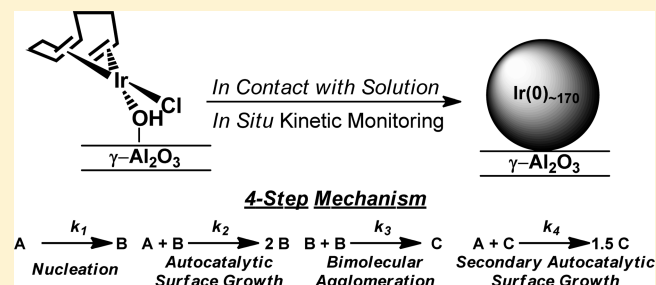
Patrick D. Kent, Joseph E. Mondloch, and Richard G. Finke*

Department of Chemistry, Colorado State University, Fort Collins, Colorado 80523, United States

Ⓢ *Supporting Information*

ABSTRACT: Product stoichiometry, particle-size defocusing, and kinetic evidence are reported consistent with and supportive of a four-step mechanism of supported transition-metal nanoparticle formation in contact with solution: slow continuous nucleation, A → B (rate constant k_1), autocatalytic surface growth, A + B → 2B (rate constant k_2), bimolecular agglomeration, B + B → C (rate constant k_3), and secondary autocatalytic surface growth, A + C → 1.5C (rate constant k_4), where A is nominally the Ir(1,5-COD)Cl/γ-Al$_2$O$_3$ precursor, B the growing Ir(0) particles, and C the larger, catalytically active nanoparticles. The significance of this work is at least 4-fold: first, this is the first documentation of a four-step mechanism for supported-nanoparticle formation in contact with solution. Second, the proposed four-step mechanism, which was obtained following the disproof of 18 alternative mechanisms, is a new four-step mechanism in which the new fourth step is A + C → 1.5C in the presence of the solid, γ-Al$_2$O$_3$ support. Third, the four-step mechanism provides rare, precise chemical and kinetic precedent for metal particle nucleation, growth, and now agglomeration (B + B → C) and secondary surface autocatalytic growth (A + C → 1.5C) involved in supported-nanoparticle heterogeneous catalyst formation in contact with solution. Fourth, one now has firm, disproof-based chemical-mechanism precedent for two specific, balanced pseudoelementary kinetic steps and their precise chemical descriptors of bimolecular particle agglomeration, B + B → C, and autocatalytic agglomeration, B + C → 1.5C, involved in, for example, nanoparticle catalyst sintering.

4-Step Mechanism

A $\xrightarrow{k_1}$ B	A + B $\xrightarrow{k_2}$ 2 B	B + B $\xrightarrow{k_3}$ C	A + C $\xrightarrow{k_4}$ 1.5 C
Nucleation	*Autocatalytic Surface Growth*	*Bimolecular Agglomeration*	*Secondary Autocatalytic Surface Growth*

■ INTRODUCTION

Establishing the mechanism(s) of supported-nanoparticle heterogeneous catalyst formation in contact with solution is essential for transferring the synthetic,[1a−i] as well as the now available mechanistic,[2−8] insights from the modern revolution in nanoparticle science in solution to the synthesis of supported-nanoparticle heterogeneous catalysts and their resultant catalysis. Despite this, kinetic and mechanistic studies of the formation of supported nanoparticle catalysts are rare, in large part (i) due to the lack of reproducible supported-nanoparticle formation systems that start from well-characterized supported-metal precatalysts, that have known reaction stoichiometries and which yield compositionally well-defined supported-nanoparticle products,[9,10] and (ii) due to the paucity of experimental methods able to follow nanoparticle formation in real time.[11−13] As result of these limitations, only a single, kinetically documented[14] mechanism has appeared in the literature for supported-nanoparticle heterogeneous catalyst formation in contact with solution.[9,10] Discovery of that mechanism relied on the development of a prototype[15] Ir(1,5-COD)Cl/γ-Al$_2$O$_3$ to Ir(0)$_{\sim900}$/γ-Al$_2$O$_3$ supported-nanoparticle heterogeneous catalyst formation system in contact with acetone and cyclohexene and its reduction under H$_2$, Scheme 1.[9]

Scheme 1. Recently Developed Ir(1,5-COD)Cl/γ-Al$_2$O$_3$ to Ir(0)$_{\sim900}$/γ-Al$_2$O$_3$ Supported-Nanoparticle Heterogeneous Catalyst Formation System in Contact with Solution[9] [a]
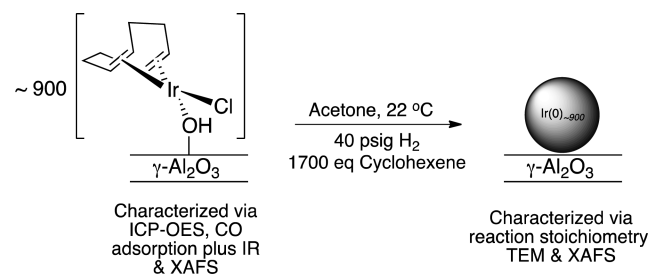
[a] The reaction begins from 0.05 g of Ir(1,5-COD)Cl/γ-Al$_2$O$_3$ in 2.5 mL of acetone and 0.5 mL of cyclohexene and is reduced under 40 psig of H$_2$.

Recent Kinetically Documented Mechanism of Supported-Nanoparticle Heterogeneous Catalyst Formation in Contact with Solution. Initial kinetic studies of the Ir(1,5-COD)Cl/γ-Al$_2$O$_3$ to Ir(0)$_{\sim900}$/γ-Al$_2$O$_3$ supported-nano-

particle formation reaction in acetone revealed sigmoidal kinetics that were well fit to a two-step mechanism of nucleation (A → B, rate constant k_1) followed by autocatalytic surface growth (A + B → 2B, rate constant k_2).[9] Subsequent kinetic and mechanistic studies demonstrated that nucleation occurs bimolecularly from Ir(1,5-COD)Cl(solvent) in solution, but that the nanoparticle growth occurs on the γ-Al$_2$O$_3$ surface with soluble Ir(1,5-COD)Cl(solvent) (i.e., A-solvate) participating in autocatalytic surface-growth of the supported nanoparticle.[10,16] To date, this two-step mechanism is the only kinetically documented mechanism for supported-nanoparticle heterogeneous catalyst formation in contact with solution.[17]

Interestingly, over the course of our (Ir(1,5-COD)Cl/γ-Al$_2$O$_3$ to Ir(0)$_{\sim 900}$/γ-Al$_2$O$_3$) kinetic and mechanistic studies, we observed kinetic curves that are significantly different than those found to be fit by the two-step mechanism, vide infra, Figure 2. That said, similar kinetic curves to those seen herein (Figures 3−6, vide infra) have been published by us as part of our studies of ligand-stabilized nanoparticle formation in solution.[4−6] Previously, such kinetic curves were fit to a four-step mechanism in solution consisting of nucleation (A → B, rate constant k_1), autocatalytic surface growth (A + B → 2B, rate constant k_2), bimolecular agglomeration (B + B → C, rate constant k_3), and autocatalytic agglomeration (B + C → 1.5C, rate constant k_4), hereafter referred to as the B+C four-step mechanism for its fourth step, where A is the organometallic precursor, B represents the intermediate, smaller nanoclusters/particles, and C represents the final, larger metal nanoparticles, Scheme 2.[4−6]

Scheme 2. Previous B+C Four-Step Mechanism for Soluble Nanoparticle Formation in Solution Where A Is the Organometallic Ir Precursor, B Represents the Small Clusters and Nanoparticles, and C Represents the Larger Nanoparticles up to Bulk Metal[a]
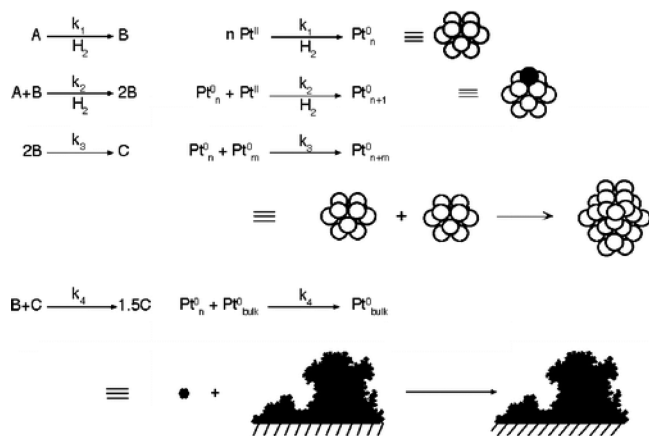
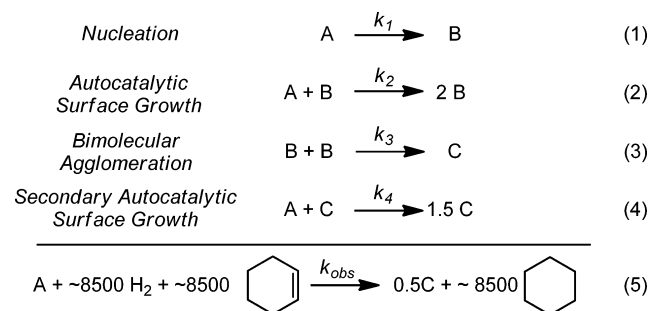[a]Reproduced from ref 4 with permission.

The key conceptual difference between the two-step mechanism and the B + B four-step mechanism is the presence of the agglomeration steps in the four-step mechanism. Hence, an important goal is to understand, and then eventually exploit synthetically, those two agglomeration steps in the preparation of the next generation of supported-nanoparticle catalysts. Noteworthy here is evidence suggesting that the larger nanoparticles, C, can be more active catalysts, apparently due to weaker metal−ligand bond energies in the larger nano-

particles as elucidated and discussed elsewhere.[4−6,18] Also noteworthy is that the B + B → C step is particle-size distribution *defocusing*, while the B + C → 1.5C autocatalytic step is particle-size distribution *focusing*. Evidence for particle-size distribution focusing come from our previous observation that when a B + C → 1.5C step is dominant, a decrease in particle-size dispersity is seen (e.g., from 21% to 7.1%).[19]

One overarching, global hypothesis for these studies is synthetic in nature, namely that the formation of well-defined supported-nanoparticle heterogeneous catalysts in contact with solution, and from supported organometallic precatalysts such as Ir(1,5-COD)Cl/γ-Al$_2$O$_3$, holds considerable potential as a relatively new, to-date little investigated, alternative method of preparing heterogeneous catalysts[20] (i.e., and compared to the much better investigated gas−solid reaction of, for example, H$_2$ reduction of a supported precatalyst). Another hypothesis is that the synthesis of supported-nanoparticles in contact with solution, from well-defined, molecular, supported precatalysts such as the prototype Ir(1,5-COD)Cl/γ-Al$_2$O$_3$ system, may prove to be an effective way to transfer at least some of the key insights, from the modern revolution in nanoparticle synthesis in solution, to the important area of supported-nanoparticle solid heterogeneous catalysts. Underpinning both of the above synthetic-chemistry-based hypothesis is the expectation that quantitative kinetic and mechanistic studies are essential for the rational, most facile, and most efficient development of heterogeneous catalyst preparations in contact with solution.

Hence, we present herein kinetic and mechanistic studies of Ir(1,5-COD)Cl/γ-Al$_2$O$_3$ to Ir(0)$_{\sim 170}$/γ-Al$_2$O$_3$ supported-nanoparticle nucleation, growth, and now agglomeration plus secondary autocatalytic surface growth. Our product and kinetic data are consistent with the aforementioned new A+C four-step mechanism shown in Schemes 3 and 4, vide infra. The

Scheme 3. Proposed A+C Four-Step Mechanism for Metal Oxide Supported-Nanoparticle Formation in Contact with Solution Named for Its Fourth A+C Step, Where A Is the Organometallic Ir Precursor, B Represents Small Clusters and Nanoparticles, and C Represents Larger, Catalytically Active Nanoparticles[a]

Nucleation	$A \xrightarrow{k_1} B$	(1)
Autocatalytic Surface Growth	$A + B \xrightarrow{k_2} 2\,B$	(2)
Bimolecular Agglomeration	$B + B \xrightarrow{k_3} C$	(3)
Secondary Autocatalytic Surface Growth	$A + C \xrightarrow{k_4} 1.5\,C$	(4)

$$A + {\sim}8500\ H_2 + {\sim}8500\ \bigcirc \xrightarrow{k_{obs}} 0.5C + {\sim}8500\ \hexagon \quad (5)$$

[a]The net reaction of A → 0.5C is coupled to fast cyclohexene hydrogenation in a cyclohexene reporter reaction,[2,4−6,9] eq 5.

resulting new mechanism, containing now two autocatalytic[21] growth steps, is the first four-step mechanism to be detailed for the formation of a metal-oxide supported-nanoparticle heterogeneous catalyst in any media (here in contact with solution). In reaching this mechanism, we have ruled out our precedented literature two-step mechanism found to be active in the previous, prototype metal-oxide work,[9,10] as well as its three-step extension which includes nanoparticle agglomeration

Scheme 4. Schematic Representation of the Steps of the A+C Four-Step Mechanism for Nanoparticle Formation and Agglomeration[a]
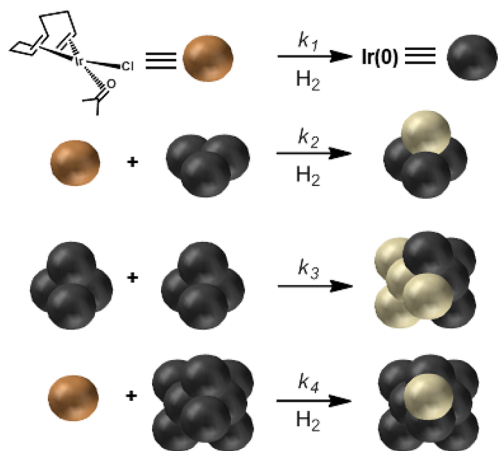
[a]Note that this scheme intentionally shows only the four steps and not if those steps occur in solution, on the metal-oxide support, or possibly in/on both. Note also that B, which represents the smaller, growing Ir(0)$_n$ clusters, is illustrated below in just three of its roles, as B = the first Ir(0)$_1$, and then in a k_2 step (somewhat arbitrarily, i.e., just for the sake of illustration) as B = Ir(0)$_3$ and then the B = Ir(0)$_4$ product of that autocatalytic step).

(B + B → 0.5 C),[3] and also the B+C four-step mechanism (i.e., with its B + C → 1.5C step) that derives from the formation of soluble, ligand-stabilized nanoparticles in solution.[4−6] Additionally, we have tested and been able to disprove 14 other possible mechanisms (as detailed in the Supporting Information); that is, we have been able to disprove 18 total alternative mechanisms, en route to settling on the A+C four-step mechanism proposed herein. As such, the evidence is that the new four-step mechanism uncovered during this work is an important finding in the literature and history of supported transition-metal nanoparticle heterogeneous catalyst formation.
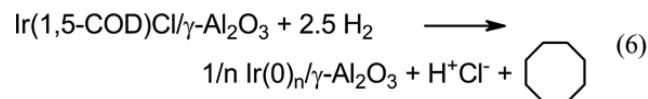
■ RESULTS AND DISCUSSION

Initial Control Experiments Verifying the Six Main Results for the Previous Prototype Two-Step System, Ir(1,5-COD)Cl/γ-Al$_2$O$_3$ to Ir(0)$_{∼900}$/γ-Al$_2$O$_3$. Prior to the present work being stated, the new researcher on this project (P.D.K.) was trained by replicating the six main results of the previous prototype, two-step formation system[9] as controls and training for the present work. The results of those six key experiments, which pleasingly reproduced completely and quantitatively the prior work (performed by J.E.M.),[9] are provided in the Supporting Information.

Ir(1,5-COD)Cl/γ-Al$_2$O$_3$ to Ir(0)$_{∼170}$/γ-Al$_2$O$_3$ Synthetic Conditions, Reaction Stoichiometry, and Resultant Products. The unusual kinetic curves (Figure 2, vide infra) were first observed when 0.010 g of the 2.0 wt % Ir(1,5-COD)Cl/γ-Al$_2$O$_3$ precatalyst was placed in 2.5 mL of acetone and 0.5 mL of cyclohexene and reduced under 40 psig of H$_2$. That is, a simple 5-fold decrease in the Ir(1,5-COD)Cl/γ-Al$_2$O$_3$ precatalyst concentration, along with the resultant 5.3 fold increase in the ratio of the cyclohexene to Ir concentrations (i.e., and vs the otherwise identical conditions used previously as shown in Scheme 1 and which led to Ir(0)$_{∼900}$/γ-Al$_2$O$_3$ via two-step kinetics[9]), yielded kinetic curves that are clearly

different and distinguishable (i.e., Figure 2, vide infra, vs Figure S4, Supporting Information).[9]

As before,[9] but now when starting from 0.010 g of the Ir(1,5-COD)Cl/γ-Al$_2$O$_3$ precatalyst, the organic 1,5-COD ligand that is part of the Ir(1,5-COD)Cl/γ-Al$_2$O$_3$ precatalyst allowed us to confirm the reaction stoichiometry via the evolution of the hydrogenated 1,5-COD product, cyclooctane, eq 6. As

$$\text{Ir(1,5-COD)Cl/}\gamma\text{-Al}_2\text{O}_3 + 2.5\ \text{H}_2 \longrightarrow$$
$$\text{1/n Ir(0)}_n/\gamma\text{-Al}_2\text{O}_3 + \text{H}^+\text{Cl}^- + \bigcirc \quad (6)$$

expected, 1.0 ± 0.1 equiv of cyclooctane per Ir evolved after approximately 6 h as confirmed via GLC. Over the course of the reaction, the initially yellow Ir(1,5-COD)Cl/γ-Al$_2$O$_3$ precatalyst turns dark gray, indicative of the formation of Ir(0)$_n$ nanoparticles.[9] The formation of 1.0 equiv of H$^+$Cl$^-$ was confirmed by a pH$_{apparent}$ measurement, Supporting Information, Figure S34. Mass balance then required the uptake of 2.5 equiv of H$_2$ as independently verified previously (and once H• spillover effects are taken into account[9]), confirming the balanced reaction stoichiometry, eq 6.

The dark-gray product produced after 6 h (i.e., after 1.0 equiv of cyclooctane had evolved by GLC, vide supra) was examined via TEM. The resultant nanoparticles are 1.7 ± 0.5 nm in diameter, corresponding on average to Ir(0)$_{∼170}$ nanoparticles supported on γ-Al$_2$O$_3$ with ±30% dispersity (as further detailed in the Supporting Information), Figure 1. Significantly,
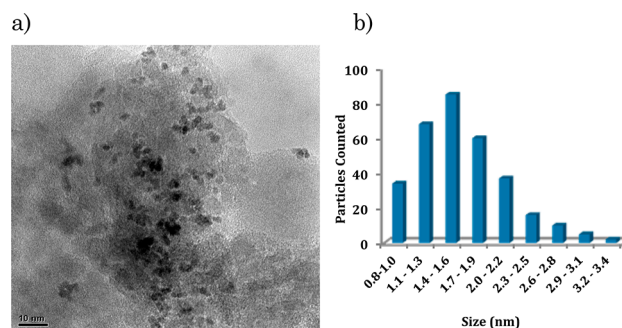

Figure 1. Sample TEM image of the supported nanoparticle product. (b) The associated particle size histogram from the resultant Ir(0)$_{∼170}$/γ-Al$_2$O$_3$ catalyst of 1.7 ± 0.5 nm average-size nanoparticles.

---

comparing these ±30% dispersion nanoparticles to the ±14% dispersion nanoparticles formed previously via the two-step mechanism (i.e., 2.9 ± 0.4 nm diameter, so-called near-monodisperse,[22] on average Ir(0)$_{∼900}$/γ-Al$_2$O$_3$ supported-nanoparticles from the two-step mechanism) reveals both smaller Ir(0)$_{∼170}$, and more polydisperse (±30% vs ±14%) nanoparticles when starting with 0.010 g Ir(1,5-COD)Cl/γ-Al$_2$O$_3$ in the present studies. We have previously observed a similar size coarsening as a result of a change from two-step to four-step nanoparticle formation kinetics. Specifically, in our studies of soluble nanoparticle formation in which 44 equiv of pyridine was added, a change from two- to four-step kinetics was observed with pyridine addition along with a change of the particle size (and dispersity) from 2.2 ± 0.3 nm (±15%) to 5 ± 2 nm (40%).[6]

Based on the preceding GLC, pH$_{apparent}$ and TEM data, the overall reaction stoichiometry for the conversion of Ir(1,5-COD)Cl/γ-Al$_2$O$_3$ to Ir(0)$_{∼170}$/γ-Al$_2$O$_3$ is given back in eq 6.

Kinetic Monitoring Method and Resultant Data. It is important to understand how the kinetic data for the $Ir(0)_n/\gamma$-Al_2O_3 supported-nanoparticle formation reaction were collected. The kinetic data are obtained indirectly, but powerfully and in real time, by the precedented cyclohexene reporter reaction method.[2−6,9,10,13] This now very well-precedented method[2−6,9,10,13] takes advantage of the fact that the metal particles, and in particular the supported-nanoparticles C in the present four-step mechanism (vide infra), are a fast cyclohexene hydrogenation catalyst. As a result, the formation of C can be followed indirectly, but in real time and under conditions where a large amount of high-precision data can be collected, via a cyclohexene hydrogenation reporter reaction,[2−6,9,10,13] as illustrated in Scheme 5. The loss of H_2 gas is followed via a

Scheme 5. Cyclohexene Reporter Reaction Employed To Follow the Formation of $Ir(0)_n/\gamma$-Al_2O_3 via the Catalytic Amplification of the Formation of the Most Active Catalyst, Which Will Turn Out To Be C[a]

$$A$$
$$\downarrow (k_{1obs}, k_{2obs})$$
$$B$$
$$\downarrow (k_{3obs}, k_{4obs})$$
$$C$$

Fast

S ... $+ H_2$
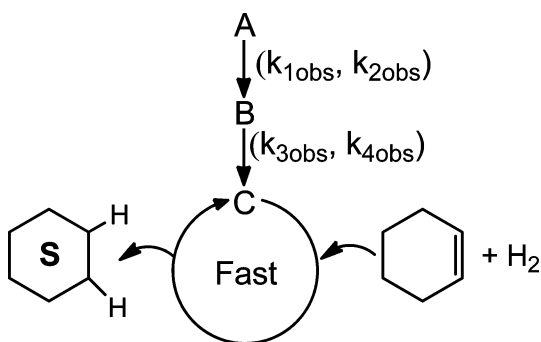
[a]Overall, the loss of H_2 or cyclohexene can be used to follow the slower kinetics of nanoparticle formation (i.e., the sequence A → B → C).

high precision (± 0.01 psig), computer-interfaced pressure transducer resulting in hundreds to thousands of high-precision kinetic data points. That H_2 loss is then, for convenience, converted by the known 1:1 H_2:cyclohexene stoichiometry[9] into cyclohexene loss which is what is plotted, as in Figure 2, vide infra. The nanoparticle nucleation, growth, and agglomeration rate constants, k_1−k_4, can then be obtained using the now well-documented pseudoelementary step technique that is central to this kinetic method[2−6,9,10,13], basically eq 5 in Scheme 3. In short, the psueodelementary step method couples fast cyclohexene hydrogenation (eq 5, vide supra) to the slower nanoparticle formation steps of the four-step mechanism, eqs 1−5, Scheme 2 vide supra.

From the kinetic fits, we find that the larger nanoparticles C are the active catalyst, not the on-average smaller particles B (vide infra). Equation 5 is the net pseudoelementary step, which in turn allows us to make the needed connection between the loss of A, the formation of the supported-nanoparticles, C, and the loss of cyclohexene, $-d[A]/dt = -d[cyclohexene]/dt = (+1/0.5)d[C]/dt$, all according to eq 5. The details of the pseudoelementary step method,[2−6,9,10,13] along with its coupling to the four-step mechanism, have been extensively documented in earlier papers.[4−6]

A Four-Step Mechanism Consistent with the Ir(1,5-COD)Cl/γ-Al_2O_3 to $Ir(0)_{\sim170}/\gamma$-Al_2O_3 Supported-Nanoparticle Heterogeneous Catalyst Formation Kinetics. The observed $Ir(0)_{\sim170}/\gamma$-Al_2O_3 supported-nanoparticle heteroge-

neous catalyst formation kinetics are very well accounted for by the A+C four-step mechanism, Scheme 3, consisting of nucleation (A → B, rate constant k_1), autocatalytic surface growth (A + B → 2B, rate constant k_2), bimolecular agglomeration (B + B → C, rate constant k_3), and secondary autocatalytic surface growth (A + C → 1.5C, rate constant k_4), Figure 2 blue line. That fit requires that the larger nanoparticles, C, be the kinetically dominant hydrogenation catalyst over the course of the supported-nanoparticle formation measurement.[23] Control fits detailed in the Supporting Information attempting to use B as the kinetically dominant form of the catalyst do not fit the observed kinetic data. The kinetic curve in Figure 2 (along with their excellent fits to the four-step
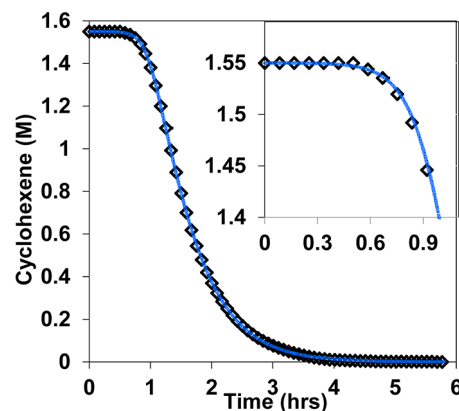

Figure 2. The nanoparticle-formation kinetics observed for Ir(15-COD)Cl/γ-Al_2O_3 to $Ir(0)_{\sim170}/\gamma$-Al_2O_3 curve-fit by the A+C four-step mechanism shown back in seen in Scheme 3. The inset shows the A+C mechanisms accounts very well for the turn-on part of the curve. For clarity, only one out of every five experimental points collected is displayed.

mechanism, $R^2 \geq 0.9999$) has been repeated 25 times, from 8 separately synthesized batches of Ir(1,5-COD)Cl/γ-Al_2O_3, across two researchers (P.D.K. and J.E.M.). No discernible variation in the global shape of the kinetic curves has been observed over these 25 experiments (although the system is sensitive to variables such as the amount of water present in the acetone solvent or the level of autoxidation impurities in the cyclohexene, and, therefore, how the cyclohexene is purified, as detailed in Experimental Section). The resultant rate constants (averages from the 25 reactions), obtained via the fits to the data are: $k_1 = 10^{-3} - 10^{-5}$ h^{-1}, $k_2 = 4.7(1) \times 10^4$ h^{-1} M^{-1}, $k_3 = 3.2(2) \times 10^5$ h^{-1} M^{-1} and $k_4 = 2.1(4) \times 10^4$ h^{-1} M^{-1}, where the numbers in the brackets are, as usual, the error in the last significant figure to 1 standard deviation. Importantly, the k_2, k_3 and k_4 rate constants have been corrected (as the math requires[4,5,9,10,13]) for the ~8500 cyclohexene stoichiometry factor of the pseudoelementary step, all as detailed previously.[4,5,9,10,13] The high relative error in the k_1 rate constant is expected (i.e., as seen before and as discussed elsewhere[5]), precise nucleation rate constants being notoriously hard to measure throughout nature.

Verifying the Reporter Reaction Kinetics. Importantly, the supported-nanoparticle heterogeneous catalyst formation kinetics, obtained via the cyclohexene reporter reaction method, were confirmed by monitoring the evolution of cyclooctane directly by GLC, Figure 3. The cyclooctane evolution data are nicely accounted for using the rate constants obtained via the cyclohexene reporter reaction (vide supra),
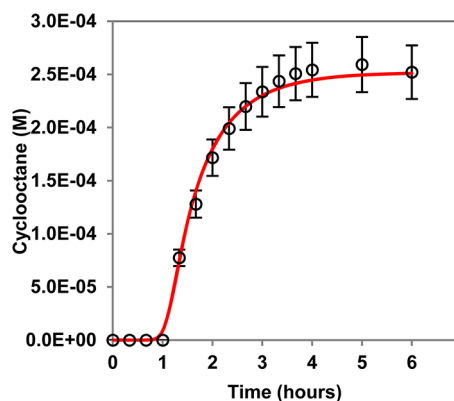
Figure 3. The production of cyclooctane from the hydrogenation of cyclooctadiene ligand as monitored by GLC and well-fit by the four rate constants that were obtained from the cyclohexene reporter reaction kinetics and curve-fitting. By 6 h, 1.0 equiv of cyclooctane per Ir had evolved consistent with and supportive of the reaction stoichiometry provided in eq 6.

results that provide independent verification of the $Ir(0)_{\sim 170}/\gamma$-Al_2O_3 supported-nanoparticle formation kinetics. In short, the $Ir(1,5\text{-COD})Cl/\gamma$-$Al_2O_3$ to $Ir(0)_{\sim 170}/\gamma$-Al_2O_3 supported-nano-particle heterogeneous catalyst formation kinetics are well accounted for by the proposed A+C four-step mechanism.

Disproof of the Two-Step and Three-Step Mechanisms. Two established[2,3] mechanisms disproven early on in this work are the two-step mechanism (i.e., just steps k_1 and k_2, Scheme 3),[9,10,13] and the three-step mechanism (i.e., steps k_1-k_3, Scheme 3).[3] Qualitatively, neither the two-step (Figure 4, vide supra, red line) nor the three-step mechanism (Figure 4,
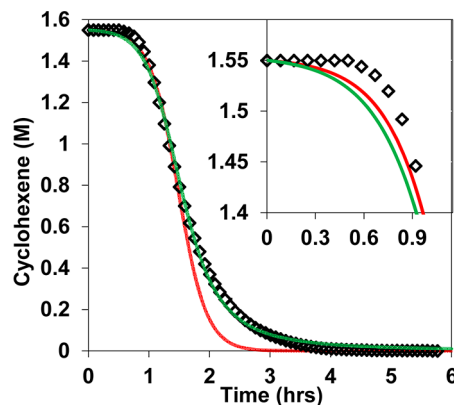

Figure 4. The nanoparticle-formation kinetics observed for the conversion of $Ir(15\text{-COD})Cl/\gamma$-$Al_2O_3$ to an $Ir(0)_{\sim 170}/\gamma$-Al_2O_3 supported-nanoparticle heterogeneous catalyst. An attempt to curve-fit the observed nanoparticle formation kinetics by the two-step mechanism is shown in red (eqs 1 and 2, Scheme 3, vide supra) and then by the three-step mechanism shown in green (eqs 1−3, Scheme 2). The inset reveals the poor fit of the turn-on portion of the curve. For clarity, only one out of every five experimental points collected in this particular experiment is displayed.

vide supra, green line) can account for the observed kinetic data, a result which we expected based on the shape of the kinetic curves and our experience with the two- and three-step mechanisms (those attempted two- and three-step mechanism fits giving relatively low R^2 values of 0.9863 and 0.9984, respectively). Furthermore, the two- and three-step mechanisms were quantitatively ruled out using Akaike's Information

Criterion (AIC), a statistical test capable of comparing models with varying numbers of parameters;[24] those statistical results are provided in the Supporting Information for the interested reader. The combined low R^2 and AIC statistics allow us to rule out the two- and three-step mechanisms in comparison to the statistically better-fitting four-step mechanism. In short, neither the two-step nor the three-step mechanism can fully account for the kinetic curves shown in Figure 2. However, a mechanism containing four steps can account quantitatively for the kinetic data, but only if a new A + C → 1.5C step is used as the fourth step of the resultant, overall new mechanism, as further discussed below.

Disproof of 14 Additional, Alternative Mechanisms. Because mechanisms are never proven and, instead, alternative mechanisms can only be disproven, it was important to consider all possible, reasonable alternative mechanisms. Relevant here is that 18 total alternative mechanisms were tested and disproven in our prior mechanistic work en route to developing the previous four-step mechanism for ligand-stabilized, solution nanoparticle formation.[4]

Fourteen of those 18 alternative mechanisms were, therefore, also tested as part of the present work. In each case they could be disproven simply by showing that they do not fit the kinetic data (see the attempted curve-fits using those 14 alternative mechanisms provided in the Supporting Information). Hence, those specific 14 possible, now disproven mechanisms need not be discussed further.

Disproving Two Alternative Four-Step Mechanisms by Following the Concentration Profile of the Ir(1,5-COD)Cl(Solvate) by UV−Visible Spectroscopy. However, two alternative four-step mechanisms *are* able to fit at least the cyclohexene reporter reaction kinetic data equally well (i.e., R^2 values ≥0.999). Interestingly but not unexpectedly, those two alternative four-step mechanisms (shown in Figure 5, Table 1,
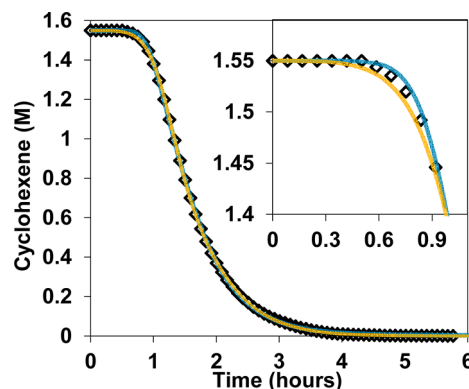

Figure 5. The hydrogenation kinetics observed for $Ir(1,5\text{-COD})Cl/\gamma$-$Al_2O_3$ to $Ir(0)_{\sim 170}/\gamma$-Al_2O_3 supported-nanoparticle heterogeneous catalyst formation curve fit by the B+C, green line, and (A,B)+C, gold line, mechanisms. The inset shows that both mechanisms can account for the turn-on feature of the kinetic curve, as expected, because they both contain two autocatalytic steps. For clarity, only one out of every five experimental points is displayed.

and detailed further in the Supporting Information) are what we denote as the following: the B+C mechanism (for its fourth step), A → B, A + B → 2B, B + B → C, and B + C → 1.5C; and the (A,B) + C mechanism (labeled for its third and fourth steps), A → B, A + B → 2B, A + C → 1.5C, and B + C → 1.5C. One key is that each of the three four-step mechanisms

Table 1. Comparison of Rate Constants for the A+C, B+C, and (A,B)+C Four-Step Mechanisms, the Precise Details and Definitions of Which Are Provided in the Main Text

Mechanism	R^2	k_1 (h^{-1})	k_{2corr} (h^{-1} M^{-1})^a	k_{3corr} (h^{-1} M^{-1})^a	k_{4corr} (h^{-1} M^{-1})^a
A + C	0.9999	10^{-3}– 10^{-5}	$4.7(1) \times 10^4$	$3.1(2) \times 10^5$	$2.1(4) \times 10^4$
B + C	0.9999	10^{-2}– 10^{-4}	$4.1(8) \times 10^4$	$2.4(6) \times 10^3$	$2.0(5) \times 10^4$
(A,B)+C	0.9998	$7.1(1.5) \times 10^{-1}$	10^0– 10^2	$1.1(3) \times 10^5$	$2.1(4) \times 10^5$

^{a}Rate constants k_2–k_4 were all corrected by a stoichiometry factor of ~8500 from the cyclohexene reporter reaction as seen in Scheme 3, eq 5.

contains two autocatalytic steps,[4−6] a crucial feature necessary to fit the reaction's sharp turn-on.

However, a second key is that there are notable differences between the three sets of rate constants k_1−k_4, reported in Table 1, obtained by fitting each of the three distinct four-step mechanisms to the identical reporter-reaction kinetic data. What this means is that there is sufficient flexibility within four rate-constant parameters to fit the distinct mechanisms to the same set of kinetic data, because that data measures, basically, the rate of formation of the catalyst, species C. This implies that if we used the three distinct sets of k_1−k_4 rate constants to create predicted A, B, and C concentration vs time profiles for each of the possible four-step mechanisms, then those profiles would probably be distinctive, as they in fact are, Figure 6, differing significantly in the loss of the Ir(1,5-COD)Cl/γ-Al$_2$O$_3$ precursor, A, and the formation of B. Hence and in turn, these three remaining four-step mechanisms should be distinguishable by following the concentration of A under the reaction conditions. Fortunately, this did prove possible, so that two of the three four-step mechanisms could be ruled out, as detailed next, leaving only the A+C four-step mechanism able to explain all of the available data, vide infra, from among the 19 total mechanisms considered.

Disproving two of the three four-step mechanisms relied upon exploiting the previous finding of a prior equilibrium in acetone in which the Ir(1,5-COD)Cl/γ-Al$_2$O$_3$ precatalyst is in a dissociative equilibrium with Ir(1,5-COD)Cl(solvent) (defined as A-solvate) and the γ-Al$_2$O$_3$ support, the A-solvate being the actual species that undergoes the nucleation step in solution in

at least the two-step mechanism of supported-nanoparticle formation.[10] Specifically and using the measured $K_{dissociation}$ in acetone,[10] only ~20% of the Ir(1,5-COD)Cl initially present in the Ir(1,5-COD)Cl/γ-Al$_2$O$_3$ remains on the support under the reaction conditions and post establishment of the prior, dissociative equilibrium (as detailed in the Supporting Information). Hence, it proved possible (as before[10]) to follow the dissociated Ir(1,5-COD)Cl(solvent) (i.e., A-solvate), by UV−vis spectroscopy of its metal-to-ligand charge transfer absorbance at 396 nm[25] and then to use that A_{396} and computed [A-solvate] to obtain the desired [A]$_{total}$ = [Ir(1,5-COD)Cl/γ-Al$_2$O$_3$] vs time.

The needed experiments were accomplished via six independent reactions which were run on a two-times scale[26] (i.e., with 0.020 g of 2.0 wt % Ir(1,5-COD)Cl/γ-Al$_2$O$_3$, in 5.0 mL of acetone and 1.0 mL of cyclohexene under 40 psig H$_2$). Each reaction was stopped at a predetermined time, brought back into the drybox, and filtered into an O$_2$-free UV−vis cell through a 0.2 μm nylon filter (to remove the alumina support). The concentration of A-solvate was then measured at six time points, with this set of experiments being repeated in triplicate. The resulting, composite spectra are available in the Supporting Information, Figure S8. Then, using the measured [A-solvate]$_{eq}$, the desired concentration of A with respect to time was determined as detailed further in the Supporting Information.

Significantly, comparing the UV−vis measurements of A_{total} to the simulated concentration profiles of A, Figure 7, shows that neither the B+C, nor the (A,B)+C, four-step mechanisms can account for the observed loss of A. These latter two, alternative four-step mechanisms are, hereby and therefore, disproven.

This leaves only the A+C mechanism as able to account for the kinetics of both the cyclohexene hydrogenation and the consumption of the precursor, A, from among the now total of 19 mechanisms tested. That A+C mechanism consists of the following steps as shown schematically in Scheme 4: nucleation (A → B, rate constant k_1), autocatalytic surface growth (A + B → 2B, rate constant k_2), bimolecular agglomeration (B + B → C, rate constant k_3), and secondary autocatalytic surface growth (A + C → 1.5C, rate constant k_4).

The first important, unprecedented result, then, is that a four-step mechanism has been discovered for metal-oxide supported-nanoparticle formation while in contact with
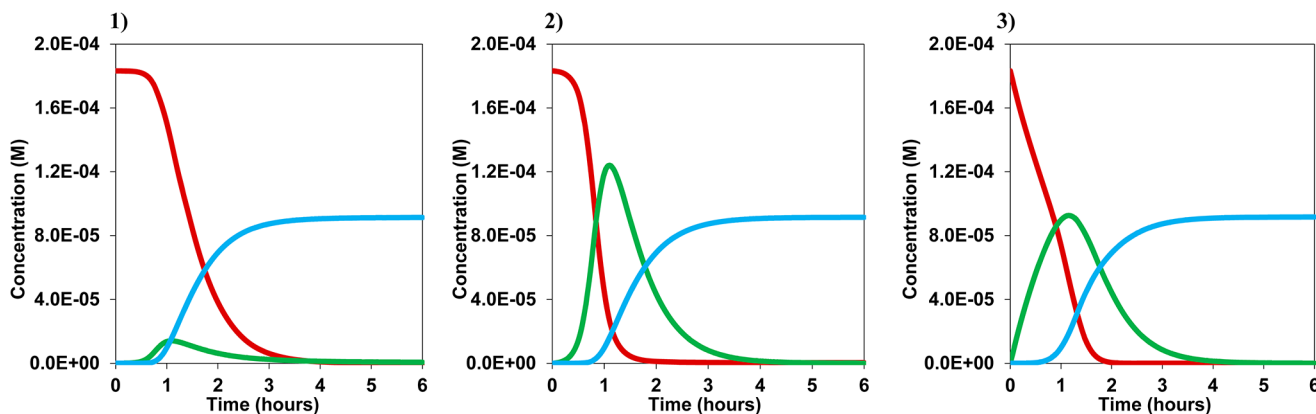

Figure 6. The concentration profiles of [A] (red line), [B] (green line), and [C] (blue line) simulated from the rate constants (k_1−k_4, Table 1) produced from curve fitting the kinetic data separately to each of the three proposed four-step mechanisms where plot 1 is A+C, plot 2 is B+C, and plot 3 is the (A,B)+C four-step mechanism.
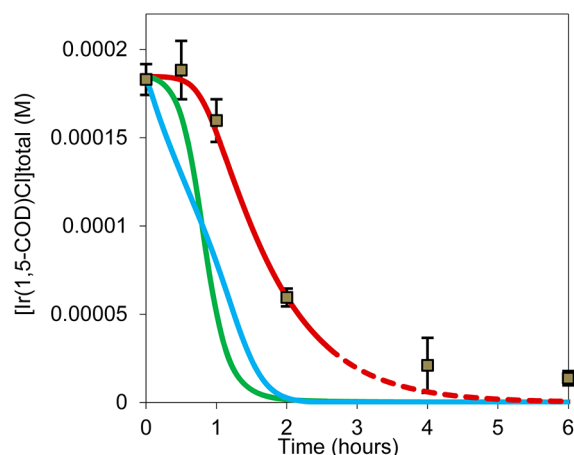
Figure 7. The concentration profiles of the Ir precursor, A, produced from the rates constants (k_1–k_4) from curve fitting separately with the three four-step mechanisms, as seen in Figure 6. The red line corresponds to A+C, the green line to B+C, and the blue line to the (A,B)+C four-step mechanism predictions for [A] vs time. Overlaid are the experimental $[A]_t$ values measured by UV−vis, results which rule out the B+C and (A,B)+C mechanisms but support the A+C four-step mechanism. The dotted lines indicate where the assumptions of zeroth order in olefin and constant hydrogen pressure in the reporter reaction breakdown significantly so that the predicted time course of A (using the four reporter-reaction measured rate constants) is no longer accurate.

solution. The second important also unprecedented result is that a new four-step mechanism has also been uncovered, namely what we have labeled herein as the "A+C" mechanism for its fourth, A + C → 1.5C step. These are not trivial findings if one looks at how little is concretely known about the mechanisms of formation of heterogeneous catalysts in terms of disproof-based chemical mechanisms consisting of precise, kinetically supported, balanced chemical reactions.[17] A third, somewhat subtle, but actually perhaps equally important result, is that precise word descriptors defined by balanced reactions are also now available in supported-nanoparticle catalyst formation, specifically nucleation, autocatalytic surface growth, bimolecular agglomeration, and secondary autocatalytic surface growth.

Limitations of the Four-Step Mechanism. As noted previously in the literature, the two-step mechanism[2] underlying the present work has several limitations that are worth emphasizing.[24,27−31] These are that the two-step and also the four-step mechanisms are as follows: (1) Ockham's razor, minimalistic kinetic models and mechanisms for nanoparticle nucleation and growth (and now agglomeration plus secondary autocatalytic surface growth); there are at least hundreds of actual elementary steps en route to the final nanoparticle products, so that the two- and four-step mechanisms are highly condensed, ultimately oversimplified, but very valuable, as they are disproof-based, Ockham's razor mechanistic models necessarily composed of the minimal number of composite, pseudoelementary steps[2] needed to fit quantitatively the observed kinetics and account for the observed products, including the increase in nanoparticle size polydispersity. (2) As such, the resultant rate constants k_1–k_4 are *averages*; indeed, all the results of the four-step model are averages of the many underlying steps. (3) Specific kinetic and mechanistic details are, then and not unexpectedly, hidden by the (otherwise kinetically quite valuable) pseudoelementary steps. For

instance, nucleation is treated in both the two- and four-step models as the precursor [A] being essentially constant throughout the nucleation stage (which it is), but this in turn means that higher kinetic orders in the nucleation step can be hidden, for example in $k_{1(apparent)}$[A]. Indeed, our recent work[16] reveals that nucleation is actually *bimolecular* as makes physical sense. What this means for the present study and resultant A+C four-step mechanism is that, in all probability, here too $k_{1(apparent)} = k_{1(true)}$[A] for the first, (bimolecular) nucleation step. This does not in any way change the value and usefulness of the observed $k_{1(apparent)}$ herein. But, the more detailed, intimate mechanism within the four-step mechanism presented herein almost surely[16,33] involves bimolecular nucleation, A + A → B, an illustration of how desirable details can be hidden kinetically in such multistep reactions until one searches for them.[16,33] (4) Similarly, the size profiles of growing intermediate and product nanoparticles are averaged and thus hidden by the general descriptors B and C, respectively, something that we are working to advance by QXAFS and other studies in progress. (5) Additionally, this lack of knowledge of the discrete size profiles of B and C also averages/hides changes in the rate constants for nucleation, growth, and agglomeration as a function of the growing nanoparticle size; it is well-known that the surface energy,[32] and number of different kinds of surface sites and defects,[33] varies as a function of nanoparticle size.[32,33] (6) Finally, both the two- and the four-step mechanisms yield only an average final particle size with no information regarding the size distribution, although they do provide the first available, mechanism-based, rigorous connection of the observed rate constants k_1 and k_2 to the final particle diameter, D_f (and for the case of the two-step mechanism).[34]

Despite these limitations that ultimately derive from the minimalistic, ultimately too simplistic, nature of the two-step mechanism, our prior four-step mechanism, and now also the new A+C four-step mechanism presented herein, these minimalistic mechanisms do presently offer the best available quantitative kinetics, disproof-based mechanisms for nanoparticle formation, now including for supported-nanoparticle formation in contact with solution.[13,24,31] As such, these mechanistic models are the necessary minimalistic kinetic models from which improvements, refinements, and more complex chemical-mechanism models can, and should be, built.

Summary, Some Additional Discussion, and Conclusions. In summary, the present study has provided product, balanced stoichiometry, kinetic, and other (i.e., GLC-monitoring of [A]) evidence in support of the first four-step mechanism for metal-oxide supported-nanoparticle formation in contact with solution. The fingerprints of the four-step mechanism include distinctive kinetic curves and a substantially defocused (±30%) product particle distribution size relative to that seen for the two-step mechanism (±14%).[9] A total of 18 alternative mechanisms were disproven en route to postulating the new A+C four-step mechanism, including ruling out two other four-step mechanisms that can fit the cyclohexene reporter reaction kinetic data (i.e., the B+C and (A,B)+C four-step mechanisms) by monitoring the profile for the loss of A. The resultant, new four-step mechanism for supported-nanoparticle formation in contact with solution is slow, continuous nucleation (A → B, rate constant k_1,[16,33] where $k_1 = k_{1(apparent)} = k_{1(true)}$[A]), autocatalytic surface growth (A + B → 2B, rate constant k_2), bimolecular agglomeration (B + B → C, rate constant k_3), and

secondary autocatalytic surface growth (A + C → 1.5C, rate constant k_4), all as shown schematically in Scheme 4.

Significantly, and in hindsight, this change in the fourth step of the mechanism, from B + C → 1.5C for soluble nanoparticle formation in solution to A + C → 1.5C for supported-nanoparticle formation in contact with solution, is readily rationalized. Specifically, the nanoparticle–support interaction appears to be limiting B's mobility and thus agglomeration ability, thereby slowing/turning off the B + C → 1.5C step on the solid support. Replacing this step kinetically is the A + C → 1.5C step (likely a solution-based A-solvate + C→1.5C step, that therefore depends on the more facile diffusion in solution of A-solvate to reach supported C for the A + C → 1.5C step). Apparently, then, diffusion limitations on the solid, γ-Al$_2$O support are implicated as a key reason for the change to a different fourth step in the resultant, new A+C four-step mechanism. The importance of diffusion limitations on solids is, in turn, fully consistent with the finding in our recent review that diffusion limitations are often present in gas–solid formation reactions of supported-nanoparticle catalysts.[17] Stated another way, one key reason to prepare supported-nanoparticle catalysts in contact with solution is to overcome such diffusion limitations inherent in many gas–solid syntheses[17], a statement consistent with, and supported by, both the literature[17] and the present studies.

Finally, the findings of this work in combination with our other four-step mechanism studies[4–6] are relevant to the agglomerative components of catalyst sintering in that they provide firm kinetic precedent for the precise kinetics of, and thus the proper names and formulations for, the bimolecular agglomeration (B + B → C) and possible autocatalytic agglomeration (B + C → 1.5C) steps in sintering. It is hard to overstate the importance of such kinetically supported, balanced chemical reaction defined, precedents as part of rigorous mechanistic work. Without them, one has collections of phenomenology grouped under descriptors for which one cannot write a balanced reaction and which, therefore, are not useful kinetically and in a rigorous mechanism. As a specific example here, the qualitative descriptor of "particle migration and coalescence (PMC)", that is nearly universally cited as one of the main two mechanisms of particle sintering,[35] is arguably now better replaced, or at least includes, bimolecular agglomeration as detailed herein, B + B → C, rate constant k_3. The second new chemical process, autocatalytic agglomeration, B + C → 1.5C, although at this point only documented in solution nanoparticle formation and agglomeration,[4–6] still provides a previously unprecedented pseudoelementary step for possible inclusion in nanoparticle sintering and even if these nanoparticles are supported on a solid oxide. The fundamental significance of the B + B → C and B + C → 1.5C pseudoelementary steps to mechanistic heterogeneous catalysis science is, conceptually, directly analogous to the fundamental significance of elementary steps to small molecule chemistry and their precise mechanisms.

Of further interest here is that the activation parameters of these agglomeration steps, at least in the case of P$_2$W$_{15}$Nb$_3$O$_{62}$[9]-stabilized Ir(0)$_{\sim900}$ nanoclusters undergoing cyclohexene hydrogenation concomitant with and agglomeration, are suggestive of associatively activated bimolecular agglomeration and dissociatively activated autocatalytic agglomeration steps (respectively, $\Delta H_3^{\ddagger} = 6.2(3)$ kcal/mol, $\Delta S_3^{\ddagger} = -46(2)$ eu and $\Delta H_4^{\ddagger} = 18(1)$ kcal/mol, and $\Delta S_4^{\ddagger} = -2.5(2)$ eu, standard state = 1 M).[36] As such, the present studies plus

those prior studies[4–6,36] are rare, precise chemical and kinetic precedent, in terms of the required balanced (pseudo)-elementary reactions with associated, explicitly defined word descriptors, for the formation, growth, and agglomeration of supported-nanoparticle heterogeneous catalysts.

Key Remaining Questions and Hence Needed Additional Kinetic and Mechanistic Studies. As in all mechanistic studies of any system with a complexity even approaching that of the present system, not all the important or interesting questions have been addressed in this first study, discovering a four-step mechanism for supported-nanoparticle formation. The needed additional studies at present include the following: (i) addressing precisely what the size profiles of B and C are vs time in the present system (a point which we have previously discussed for our soluble, ligand-stabilized nano-particle formation systems[4,5]), and then (ii) following the concentration vs time profiles for [A] and [B] directly, in principle via in operando X-ray absorbance fine structure for example, efforts in progress via our XAFS collaboration with Prof. A. Frenkel. Additional key questions include the following: (iii) what, precisely, causes the observed change from the two-step to the four-step mechanism? Our present studies suggest that perhaps *both* the lower concentration of Ir(1,5-COD)Cl/γ-Al$_2$O$_3$ plus the larger 8500 ratio of cyclo-hexene to Ir (i.e., and any remaining, insidious autoxidation or other impurities in the cyclohexene) may be key to turning on the four-step mechanism; the needed additional studies are in progress. Further questions of interest are the following: (iv) can additional insight be obtained as to why and how the presence of the solid support changes the fourth step of the four-step mechanism from B + C → 1.5C (in solution) to A + C → 1.5C when the solid, γ-Al$_2$O$_3$ support is present? Insight into questions iii and iv can likely be obtained by (iv) elucidating which steps of the new four-step mechanism are occurring in solution vs on the analogous solid by studying (as we were able to recently do in our previous work on the prototype system and its two-step mechanism[10]) the [Al$_2$O$_3$] and [solvent] dependence[10] of each step of the four-step mechanism. These and other needed additional studies are continuing and will be reported in due course.

■ EXPERIMENTAL SECTION

Prefacing Statement. Because precise, exactly worded experimental sections are essential for reproducible science, and because of the difficulty of writing experimental sections that have all the needed details in areas where the chemistry is sensitive to the precise conditions and those exact details,[37,38] in what follows we have in some sections that deliberately contain some of the same precise and careful wording we developed previously as part of this overall project.[9,10] That is, in what follows, our emphasis is on precisely worded, repeatable experimental details regardless of whether that precise experimental wording has appeared previously in any of the experimental sections of our prior 2010[9] or 2011[10] papers (i.e., in which the 2 wt % Ir(1,5-COD)Cl/γ-Al$_2$O$_3$ precatalyst employed therein is also used herein, albeit under different specific conditions in the present work).

Initial Control Experiments Verifying the Six Main Results for the Previous Two-Step System. The details and results of these controls are provided in the Supporting Information.

Materials. All solvents and compounds used were stored in the drybox prior to use. Used as received (all of which came sealed under N$_2$) were acetone (Burdick & Jackson, water content <0.5%; Aldrich, Chromasolv for HPLC, water content <0.5%), anhydrous cyclohexane (Aldrich, 99.5%), and [Ir(1,5-COD)Cl]$_2$ (STREM, 99%). Cyclo-hexene (Aldrich, 99%) was freshly distilled over Na metal or CaH,

under N_2. In our early work, cyclohexene was purified using an activated γ-Al_2O_3 column under N_2 in a MicroSolv solvent purification system (Innovative Technology). In some cases, results outside the normal range of reproducibility of the kinetics (and as described in the main text) were seen using cyclohexene prepared using the MicroSolv system (i.e., as an inherently safer method than distilling cyclohexene from for example Na). GLC of cyclohexene prepared this way (i.e., and when a single bottle of uninhibited cyclohexene was left in the system over a 3-year period) showed autoxidation products (see the Supporting Information for the GLC trace). Hence, we returned to purifying cyclohexene by distillation from Na or CaH_2 and recommend that method. Noteworthy here is that the MicroSolv system is not designed to remove at least larger amounts of peroxides. Hence, one needs to be aware that having readily autoxidized, uninhibited cyclohexene in contact with a metal container (i.e., that can serve as a catalyst for the radical-chain autoxidation of cyclohexene) is inviting formation of >70 known products of cyclohexene autoxidation if higher levels of autoxidation are achieved.[39] Regular changing of the bottle of cyclohexene, being sure the system is under N_2 pressure, and regular GLC monitoring of the purified cyclohexene product should all be performed if one chooses to use the MicroSolv system for cyclohexene purification, which, again and ultimately, we do *not* recommend.

Ethyl acetate (Aldrich, ≥99.8%, <0.05% H_2O) was degassed prior to use in the drybox. Acidic activated γ-Al_2O_3 (Aldrich), with a surface area of 155 m^2/g, was dried at 160 °C in air for 24 h. We have previously shown that additional drying of the γ-Al_2O_3 at higher temperatures, up to 500 °C,[10] has no effect on at least the two-step system.[9] H_2 gas purchased from Airgas (>99.5% purity) was passed through O_2- and H_2O-scavenging traps (Trigon Technologies) before use. All glassware used was rinsed with 18 MΩ water five times before drying at 160 °C for at least 48 h, followed by cooling under vacuum in the drybox antechamber prior to being brought into the drybox. These cautions are intended to limit the amount of residual, adsorbed water, given that water (and the associated amount of surface hydroxyl groups for example) is well-known to influence oxide-supported heterogeneous catalysts.[40]

Analytical Instrumentation and Procedures. Unless otherwise reported all reaction solutions were prepared under O_2- and moisture-free conditions in a Vacuum Atmospheres N_2-filled drybox. The O_2 level (always ≤5 ppm, typically ≤1 ppm) was continuously monitored by a Vacuum Atmospheres O_2 sensor. Gas−liquid chromatography (GLC) for cyclooctane determination was performed using a Hewlett-Packard 5890 Series II chromatograph, equipped with a flame-ionization detector and a Supelco SPB-1 (Aldrich, 30 m × 0.25 mm × 0.25 μm) fused silica column. The GLC parameters were as follows: initial oven temperature, 50 °C; initial time, 3.0 min; rate, 10 °C/min; final temperature, 160 °C; injector temperature, 180 °C; detector temperature, 200 °C; injection volume, 2 μL. GLC for the detection of autoxidation products in cyclohexene used the same column and followed the same protocols. GCMS results were obtained on a Agilent 5973N Mass Selective Detector utilizing an electron ionization source interfaced to a 6890 Gas Chromatograph which is equipped with a 7683 Automatic Liquid Sampler and Supelco SPB-1 (Aldrich, 30 m × 0.25 mm × 0.25 μm) fused silica column. UV−vis spectroscopy experiments were run on a Hewlett-Packard 8452A diode array spectrophotometer, and the data were analyzed via Hewlett-Packard's UV−vis ChemStation software. Transmission electron microscopy (TEM) analysis was conducted either at Clemson University with the expert assistance of JoAn Hudson and her staff or at Colorado State University with the expert assistance of Shannon C. Riha.

Precatalyst Preparation. All of the precatalysts were prepared in a drybox using preselected $[Ir(1,5\text{-}COD)Cl]_2$/metal oxide weight-to-weight ratios. Specifically, a 2.0% weight-to-weight $Ir(1,5\text{-}COD)Cl/\gamma$-$Al_2O_3$ sample was prepared by adding 1.0 g of predried (vide supra) acidic γ-Al_2O_3 to 20 mg of $[Ir(1,5\text{-}COD)Cl]_2$ corresponding to a 2.0 wt % sample (i.e., and where wt % = [wt $[Ir(1,5\text{-}COD)Cl]_2$/(wt $[Ir(1,5\text{-}COD)Cl]_2$+ wt γ-Al_2O_3)] × 100, as this is what we experimentally measure out and, hence, know).

More specifically, the following procedure was used. The appropriate amount of $[Ir(1,5\text{-}COD)Cl]_2$ was weighed out in a 20 mL scintillation vial. A new 5/8 in. × 5/16 in. Teflon-coated octagon-shaped stir bar was added to the vial, and the solid was dissolved in 15 mL of ethyl acetate (from Aldrich, ≥99.8%, <0.05% H_2O; the source and purity of the EtOAc proved important for reproducible precatalyst synthesis, as detailed further in the Supporting Information). Subsequently, the appropriate amount of solid oxide (e.g., 1.0 g of acidic γ-Al_2O_3 for the 2.0 wt % Ir catalyst) was added by pouring the metal oxide into the vial (i.e., this order of addition is both deliberate and important[9]), and the solution was stirred for 24 h to equilibrate the $[Ir(1,5\text{-}COD)Cl]_2$ with the solid oxide and the solution. After the 24 h equilibration period, the slurry was taken to dryness in the drybox by placing the sample under vacuum for 8 h at room temperature. The resulting 2.0% $Ir(1,5\text{-}COD)Cl/\gamma$-$Al_2O_3$ precatalyst was stored in the drybox in a sealed bottle.

Hydrogenation Apparatus and Data Handling. Hydrogenation experiments for monitoring the H_2 reduction of $Ir(1,5\text{-}COD)Cl/$ γ-Al_2O_3 to $Ir(0)_n/\gamma$-Al_2O_3 were carried out in a previously described apparatus[2−6] built to continuously monitor H_2 pressure loss. Briefly, the apparatus consists of a Fisher-Porter (FP) bottle modified with Swagelock TFE-sealed Quick-Connects to both a H_2 line and an Omega PX621 pressure transducer. The pressure transducer is interfaced to a PC through an Omega D1131 5 V A/D converter with a RS-232 connection. Reactions were run at a constant temperature by immersing the FP bottle in a 500 mL jacketed reaction flask containing dimethyl silicon fluid (Thomas Scientific), which is regulated by a thermostatted recirculating water bath (VWR). Pressure uptake data were collected using LabView 7.1. The hydrogen uptake curves were converted to cyclohexene (M) curves using the previously established 1:1 H_2/cyclohexene stoichiometry.[2,41] The data were also corrected for the acetone solvent vapor pressure using the previously established protocols[42] in which one either measures the acetone vapor pressure independently (and then subtracts that curve, point-by-point, from the raw H_2 uptake data from the cyclohexene reporter reaction data), or where one simply back-extrapolates the experimental vapor pressure rise (seen in the induction period of the reaction). Both curve-fitting methods yielded the same k_1−k_4 rate constants within ±15% for k_2−k_4 (the inherent error for k_1 is larger, as discussed in the main text).

"Standard Conditions" Supported-Nanoparticle Heterogeneous Catalyst Formation. In a drybox a "standard conditions" four-step hydrogenation was prepared and performed as follows: the appropriate precatalyst (e.g., 0.010 g of the 2.0 wt % $Ir(1,5\text{-}COD)Cl/$ γ-Al_2O_3) was weighed into a 2 dram vial and transferred to a culture tube. To ensure quantitative transfer, 2.5 mL of acetone and 0.5 mL of purified cyclohexene were added to the 2 dram vial. The solution was then transferred via a disposable polyethylene pipet into a new borosilicate culture tube (22 × 175 mm) with a new 5/8 in. × 5/16 in. Teflon-coated octagon-shaped stir bar. The culture tube was sealed in the FP bottle, removed from the drybox, and attached to the H_2 line. The sealed, H_2-line-attached FP bottle was then placed into a temperature-regulated water bath set at 22.0 ± 0.1 °C. A standard conditions purge cycle[2,41] was used to initiate the reaction. Specifically, a series of H_2-flushing cycles was performed in which the FP bottle was purged with H_2 every 15 s until 3.5 min had passed (a total of 14 purges). The stir plate was started at 600 rpm to allow the H_2 gas-to-solution equilibrium, and the H_2 pressure was then set to 40 psig, with the data recording started 4 min after H_2 was admitted into the FP bottle (i.e., by definition $t = 0$ for the kinetics).

Observed Sensitivity of the Present Four-Step Mechanism System to Solvent and Olefin Autoxidation Impurities. Over the course of the three years of these experiments, we have observed some variation in the curve-fit-obtained rate constants while changing between different suppliers of acetone and cyclohexene and also depending on how the cyclohexene was purified. The main sources of the variability in the rate constants (as detailed in the Supporting Information) seems to be differing amounts of water in the solvent (e.g., when changing from Burdick & Jackson to Aldrich acetone) and autoxidation impurities in the cyclohexene (i.e., and therefore as a

function of how the cyclohexene is purified, initially over an Al_2O_3 column vs subsequently by distillation over CaH or Na, this latter method again being what we recommend). Noteworthy here is that, under the conditions herein and where the four-step mechanism is seen, the ratio of cyclohexene to iridium (i.e., while employing the cyclohexene reporter reaction kinetic method) is 8500 and thus substantially larger than the ratio of 1600 in our previous work[10] where two-step kinetics are seen. That larger 8500 ratio makes the current system more sensitive to water or to cyclohexene autoxidation impurities detected by GLC (see the Supporting Information for details).[9,10,13]

The larger 8500 ratio of cyclohexene:Ir raised the hypothesis that this larger ratio might be the cause of the change from two- to four-step kinetics. However, a control experiment reported in the Supporting Information shows that using larger 4000 or 8500 ratios of cyclohexene:Ir under otherwise two-step conditions does not change the kinetics to four-step kinetics (i.e., two-step kinetics are still seen; see the Supporting Information, Figure S29). Hence, that hypothesis is disproven.

We have previously detailed that the nucleation k_1 value of the B+C four-step mechanism for soluble nanoparticle formation can be especially variable (observed variations of up to $\pm 10^4$)[5] while the in the present work k_1 was observed to vary up to $\pm 10^3$ over the course of the 3 years of experiments by two different experimentalists (P.D.K. and J.E.M.). The basic system has otherwise proven quite reproducible, however (as have the six main experimental observations by one of us (J.E.M.) in our prior work[10] which proved fully reproducible by another one of us (P.D.K.) as early training and control experiments at the start of the project; see the Supporting Information for a full list and the details of those six experiments.)

One other note here: during this project, we observed a period where solid, light yellow Ir(1,5-COD)Cl/γ-Al$_2$O$_3$ precatalyst visually changed to dark gray while stored (in a capped bottle) in the drybox, a color change that correlated with greatly shortened induction periods (to near zero) as if some Ir(0) catalyst was already present. Eventually, we traced this at least most plausibly to the use of BEt$_3$ in our drybox as part of a different project; once the BEt$_3$ reductant was removed from the drybox, the observed precatalyst "autoreduction" problem (as that collection of phenomena is called in the heterogeneous catalysis literature[43]) ceased. We also observed a sensitivity of the Ir(1,5-COD)Cl/γ-Al$_2$O$_3$ precatalyst to the EtOAc used in its preparation; those data are also provided as part of the Supporting Information. In short, care and attention to the purities of all reagents and other details are important to achieve the reproducible supported-nanoparticle catalyst formation reported herein.

MacKinetics Curve Fitting. The supported-nanoparticle heterogeneous catalyst formation curves (e.g., Figure 2) were fit at least initially via numerical integration using the free software MacKinetics (version 0.9.1b, by Walter S. Leipold III[44]). Details of the fitting procedure have been described previously in detail.[4] Briefly, the cyclohexene vs time curves are used as is (i.e., as described in Hydrogenation Apparatus and Data Handling) when fit with the two- and three-step mechanisms. Alternatively, data fit to the four-step mechanism were converted to 1/2 ([cyclohexene]$_0$ − [cyclohexene]$_t$) data (i.e., cyclohexene kinetic curves in terms of the product [C]). To avoid reporting local minima as a result of the numerical integration fitting,[45] an extended scan of the parameter surface (i.e., k_1−k_4) vs residual was conducted. Specifically, for each reaction, the four kinetic parameters (k_1−k_4) were varied over 4 orders of magnitude using a minimum of 10 equally spaced search points within that 10^4 range for each parameter. If the best fit of that grid search yielded a value at the limit of the grid, the grid was shifted and the search performed again.

Copasi Curve Fitting. Following the above curve fitting in MacKinetics, some data were also refit in Copasi 4.8 (Build 35)[46] for comparison to the MacKinetics results. All data were prepared as outlined above, except that rather than performing a grid search, the rate constants (k_1−k_4) were estimated using the particle swarm method with an iteration limit of 2000 and a swarm size of 2000 with bounds of 0−1000. All reported rate constants refit by Copasi agreed well with the MacKinetics-determined rate constants to within ±5%,

thereby providing confidence in both the Copasi and MacKinetics curve fittings.

GLC Cyclooctane Evolution Kinetics and Determination of the Ir(1,5-COD)Cl/γ-Al$_2$O$_3$ Reaction Stoichiometry. The procedure employed was very similar to that previously published.[9] In a drybox, 0.01 g of the Ir(1,5-COD)Cl/γ-Al$_2$O$_3$ catalyst precursor was weighed into a 2 dram vial. The Ir(1,5-COD)Cl/γ-Al$_2$O$_3$ precatalyst was transferred into a new borosilicate culture tube (22 × 175 mm) with a new 5/8 in. × 516 in. Teflon-coated octagon-shaped stir bar. To ensure quantitative transfer, 2.5 mL of acetone, 0.5 mL of cyclohexene, and 2 μL of decane (as an internal standard) were added to the 2 dram vial. The solution was then thoroughly mixed and transferred via a disposable polyethylene pipet into the culture tube containing the Ir(1,5-COD)Cl/γ-Al$_2$O$_3$ precatalyst. A standard conditions hydrogenation was started (vide supra). At predetermined times, the stirring was stopped, the H$_2$ pressure was released from the FP bottle (but keeping a positive H$_2$ pressure of ≥10 psig), and aliquots (≤0.1 mL) of the reaction solution were drawn with a 9 in. needle attached to a gastight syringe. After the aliquot was drawn, the FP bottle was resealed, stirring was restarted at 600 rpm, and the FP bottle was purged five times (once every 5 s) and then allowed to fill to 40 psig (30 s). Before each aliquot was drawn, the needle was rinsed with acetone 10 times and then thoroughly dried with compressed air.

pH$_{apparent}$ Measurements Confirming the Evolution of 1.0 H$^+$Cl$^-$, Thereby Supporting the Reaction Stoichiometry. The evolution of 1 equiv of H$^+$Cl$^-$ per Ir atom was measured to further support the reaction stoichiometry, eq 6. This experiment followed the procedure used previously for quantifying the pH from the nanoparticle formation.[13] Specifically, following a standard conditions hydrogenation, the excess H$_2$ pressure was released and the FP bottle was returned to the drybox. The solution was transferred into a 20 mL scintillation vial, and the reaction culture tube was washed with 5.5 mL of acetone. The solution was then removed from the drybox, and an additional 0.5 mL of nanopure H$_2$O was added. The pH$_{apparent}$ was then measured with stirring for 1 min followed by 5 min of standing to allow the probe to equilibrate. As a blank, pH$_{apparent}$ measurements were also performed on solutions consisting of (i) 9.8 mg of Al$_2$O$_3$, 2.5 mL of acetone, 0.5 mL of cyclohexane, 5.5 mL of acetone and 0.5 mL of H$_2$O, and also on (ii) a 1.0 equiv HCl standard solution consisting of the 9.8 mg of Al$_2$O$_3$, 2.5 mL of acetone, 0.5 mL of cyclohexene, 5.5 mL of acetone, and 0.5 mL of H$_2$O containing 1 equiv of added HCl. The results of the three pH$_{apparent}$ experiments are given in the Supporting Information, Figure S34

GLC Determination of the Level of Autoxidation Impurities in Cyclohexene Purified by Three Different Methods. Following the problems with cyclohexene autoxidation occurring in the Al$_2$O$_3$-column purification system, new batches of cyclohexene were freshly distilled over CaH or Na and under N$_2$. The samples of the differently purified cyclohexenes were sealed in crimp-top vials in the drybox prior to their analysis by GLC and GCMS to prevent exposure to air. The vials were removed from the drybox, and aliquots were taken through the septum for GLC and GCMS analysis. The results are provided in the Supporting Information.

Preparation of TEM Grids. Following a standard conditions supported-nanoparticle formation reaction, and after 1.0 equiv of cyclooctane per Ir had evolved as demonstrated by GLC (vide supra), the FP bottle was transferred into the drybox. The reaction solution was placed in a 20 mL scintillation vial and diluted 2-fold (i.e., an additional 3.0 mL of acetone was added). A 300 mesh Formvar-coated SiO$_2$ TEM grid was dipped into the solution containing the Ir(0)$_n$/γ-Al$_2$O$_3$ sample for approximately 5 s and then allowed to dry. The grid was placed in a 2 dram vial and kept wax-sealed (under N$_2$) until TEM analysis.

Reaction Monitoring of the A_{total} via A-solvate by UV−Visible Spectroscopy. To distinguish between the three proposed four-step mechanisms, UV−vis was employed to follow the concentration of the Ir(1,5-COD)Cl(solvent) = A-solvate species throughout the reaction and relate that back to the desired A_{total} vs time. To fully fill the UV−vis cell, all UV−vis experiments were run at two times the standard conditions scale, that is, using 20.0 mg of the 2

wt % Ir(1,5-COD)Cl/γ-Al$_2$O$_3$ precatalyst, in 5.0 mL of acetone and 1.0 mL of cyclohexene. To ensure that scaling the reaction conditions did not alter the observed kinetics, a control hydrogenation was performed (details provided in the Supporting Information); that two-times scale control reaction yielded rate constants within experimental error for both the standard conditions and 2-fold higher scale, showing that using the 2-fold higher scale is not introducing any artifacts into the A-solvate analysis. Two-times scale catalyst formation hydrogenations were prepared by weighing 20.0 mg of precatalyst in a 20 mL scintillation vial prior to transferring to a new, clean borosilicate culture tube containing a new 5/8 in. × 5/16 in. Teflon-coated octagon-shaped stir bar. Subsequently, 5.0 mL of acetone and 1.0 mL of purified cyclohexene were added to the scintillation vial and then transferred to the culture tube via a polyethylene pipet. An otherwise standard conditions hydrogenation was then started as outlined above. Subsequently, reactions were stopped at predetermined times by releasing H$_2$ pressure and brought back into the drybox, and the solution was filtered through a 0.2 μm nylon filter in an O$_2$ free UV−vis cell, after which the UV−vis spectrum was taken at each predetermined time point.

■ ASSOCIATED CONTENT

Ⓢ Supporting Information

Training controls of the six main two-step experiments performed by P.D.K.; the B+C and (A,B)+C four-step mechanisms; curve-fits, and Akaike's Informaation Criterion analysis leading to disproof of the two-step and three-step mechanisms; the control hydrogenation at two-times scale and four-step conditions; composite UV−vis [A-solvate] spectra; derivation of the prior-equilibrium for [A-solvate]; the 14 alternative mechanisms and their disproof; GLC and GC-MS analysis of autoxidation impurities in cyclohexene; water content in ethyl acetate affecting the kinetics; a test to determine if only the larger 8500:1 cycloehexene:Ir ratio changes two-step kinetics to four-step kinetics; and pH$_{apparent}$ measurements to support the reaction stoichiometry. This material is available free of charge via the Internet at http://pubs.acs.org

■ AUTHOR INFORMATION

Corresponding Author
rfinke@lamar.colostate.edu

Notes
The authors declare no competing financial interest.

■ ACKNOWLEDGMENTS

■ REFERENCES

(1) Some recent reviews describing the synthesis of transition-metal nanoparticles include (also see the extensive references therein for additional earlier and important nanoparticle reviews): (a) Aiken, J. D., III; Finke, R. G. *J. Mol. Catal. A: Chem.* **1999**, *145*, 1. (b) Crooks, R. M.; Zhao, M.; Sun, L.; Chechik, V.; Yeung, L. K. *Acc. Chem. Res.* **2001**, *34*, 181. (c) Bönnemann, H.; Richards, R. M. *Eur. J. Inorg. Chem.* **2001**, 2455. (d) Roucoux, A.; Schulz, J.; Patin, H. *Chem. Rev.* **2002**, *102*, 3757. (e) Cushing, B. L.; Kolesnichenko, V. L.; O'Connor, C. J. *Chem. Rev.* **2004**, *104*, 3893. (f) Astruc, D.; Lu, F.; Aranzaes, J. R. *Angew. Chem., Int. Ed.* **2005**, *44*, 7852. (g) Wilcoxon, J. P.; Abrams, B. L. *Chem. Soc. Rev.* **2006**, *35*, 1162. (h) Ott, L. S.; Finke, R. G. *Coord. Chem. Rev.* **2007**, *251*, 1075. (i) Semagina, N.; Kiwi-Minsker, L. *Catal. Rev.: Sci. Eng.* **2009**, *51*, 147.

(2) Watzky, M. A.; Finke, R. G. *J. Am. Chem. Soc.* **1997**, *119*, 10382 (see also the table in the Supporting Information with the 19 prior key papers, which constituted the nanoparticle formation mechanism literature, prior to 1997.

(3) Hornstein, B. J.; Finke, R. G. *Chem. Mater.* **2004**, *16*, 139 (see also *Chem. Mater.* **2004**, *16*, 3972).

(4) Besson, C.; Finney, E. E.; Finke, R. G. *J. Am. Chem. Soc.* **2005**, *127*, 8179.

(5) Besson, C.; Finney, E. E.; Finke, R. G. *Chem. Mater.* **2005**, *17*, 4925.

(6) Finney, E. E.; Finke, R. G. *Chem. Mater.* **2008**, *20*, 1956.

(7) A recent review of the kinetic and mechanistic studies of transition-metal nanoparticle nucleation and growth, with an emphasis on the nucleation step is Finney, E. E.; Finke, R. G. *J. Colloid Interface Sci.* **2008**, *317*, 351.

(8) Some additional references, to the growing mechanistic insights into the synthesis of transition metal nanoparticles from the modern revolution in nanoparticle science presently in solution, include: (a) Zheng, H.; Smith, R. K.; Jun, Y.-W.; Kisielowski, C.; Dahmen, U.; Alivisatos, A. P. *Science* **2009**, *324*, 1309. (b) Murray, C. B. *Science* **2009**, *324*, 1276. (c) Harada, M.; Inada, Y. *Langmuir* **2009**, *25*, 6049. (d) Polte, J.; Ahner, T. T.; Delissen, F.; Sokolov, S.; Emmerling, F.; Thunemann, A. F.; Kraehnert, R. *J. Am. Chem. Soc.* **2010**, *132*, 1296. (e) Polte, J.; Erler, R.; Thunemann, A. F.; Sokolov, S.; Ahner, T. T.; Rademann, K.; Emmerling, F.; Kraehnert, R. *ACS Nano* **2010**, *4*, 1076. (f) Yao, T.; Sun, Z.; Li, Y.; Pan, Z.; Wei, H.; Xie, Y.; Nomura, M.; Niwa, Y.; Yan, W.; Wu, Z.; Jiang, Y.; Liu, Q.; Wei, S. *J. Am. Chem. Soc.* **2010**, *132*, 7696.

(9) Mondloch, J. E.; Wang, Q.; Frenkel, A. I.; Finke, R. G. *J. Am. Chem. Soc.* **2010**, *132*, 9701.

(10) Mondloch, J. E.; Finke, R. G. *J. Am. Chem. Soc.* **2011**, *133*, 7744.

(11) Chupas, P. J.; Chapman, K. W.; Jennings, G.; Lee, P. L.; Grey, C. P. *J. Am. Chem. Soc.* **2007**, *129*, 13822.

(12) Uzun, A.; Gates, B. C. *Angew. Chem., Int. Ed.* **2008**, *47*, 9245.

(13) Mondloch, J. E.; Yan, X.; Finke, R. G. *J. Am. Chem. Soc.* **2009**, *131*, 6389.

(14) See ref 26 in our earlier work and our prior review of the state-of-the-art of mechanistic knowledge of supported-nanoparticle heterogeneous catalyst formation reactions.[10,17]

(15) The eight prototype criteria previously developed[9] are (i) a compositionally and structurally well-defined supported precatalyst (accomplished previously via inductively coupled plasma optical emission spectroscopy and CO/IR trapping experiments as well as X-ray absorbance fine structure (XAFS) spectroscopy[9]), (ii) a system in contact with solution and formed under low temperature conditions, and (iii) a system where cyclooctane evolution and H$_2$ uptake studies establish the balanced stoichiometry of the supported-nanoparticle formation reaction (e.g., Scheme 3 previously confirmed[9]), leading to a well defined Ir(0)$_{\sim 900}$/γ-Al$_2$O$_3$ supported-nanoparticle heterogeneous catalyst (confirmed for the present system by TEM and XAFS[9]). In addition, a prototype system should (iv) yield an active and long-lived catalyst and hence (v) provide a system where the initial kinetic and mechanistic studies of the in situ catalyst formation are well worth the effort. Lastly, (vi) reproducible and quantitative kinetic data should result so that quantitative conclusions and mechanistic insights can be drawn, and (vii) comparison to a kinetically and mechanistically well-studied nanoparticle formation system in solution should ideally also be possible for the insights which that comparison should allow.[10]

(16) Mondloch, J. E.; Finke, R. G. *ACS Catal.* **2012**, *2*, 298.

(17) Mondloch, J. E.; Bayram, E.; Finke, R. G. *J. Mol. Catal. A: Chem.* **2012**, *355*, 1.

(18) Murzin, D. Y.; Simakova, I. L. *Catal. Lett.* **2011**, *141*, 982.

(19) Finney, E. E.; Shields, S. P.; Buhro, W. E.; Finke, R. G. *Chem. Mater.* **2012**, *24*, 1718.

(20) Traditionally, supported-nanoparticle heterogeneous catalyst syntheses have been carried out at the gas−solid interface. The present contribution is, in contrast, concerned with the supported-nanoparticle formation at the liquid−solid interface. For leading references to prior

1940

dx.doi.org/10.1021/ja410194r | *J. Am. Chem. Soc.* 2014, 136, 1930−1941

examples of supported-nanoparticle heterogeneous catalyst syntheses in contact with solution, see footnote 50 in our previous publication.[9]

(21) See footnote 20 in our earlier work for prior studies regarding double or tandem autocatalysis.[5]

(22) "Near monodisperse" nanoparticles are defined as ≤15% size distributions; see Aiken, J. D., III; Lin, Y.; Finke, R. G. *J. Mol. Catal. A: Chem.* **1996**, *114*, 29.

(23) As seen in the Supporting Information, treating B as the active hydrogenation catalyst in any of the four-step mechanisms does not result in good fits to the kinetic data. Specifically, when B is the catalyst, the fit is unable to account for the sharp turn-on in catalytic activity, undercutting the data.

(24) Finney, E. E.; Finke, R. G. *Chem. Mater.* **2009**, *21*, 4468.

(25) Epstein, R. A.; Geoffroy, G. L.; Keeney, M. E.; Mason, W. R. *Inorg. Chem.* **1979**, *18*, 478.

(26) As a control, a 2-times scale hydrogenation was run and observed to give the same rate constants within experimental error as a normal, standard conditions hydrogenation. The hydrogenation and its rate constants are reported in the Supporting Information. This control shows that no artifact is introduced by the 2-fold higher scale needed to bring the [A-solvate] into a more conveniently and accurately measured range.

(27) Morris, A. M.; Watzky, M. A.; Agar, J. N.; Finke, R. G. *Biochemistry* **2008**, *47*, 2413.

(28) Watzky, M. A.; Morris, A. M.; Ross, E. D.; Finke, R. G. *Biochemistry* **2008**, *47*, 10790.

(29) Morris, A. M.; Finke, R. G. *Biophys. Chem.* **2009**, *140*, 9.

(30) Morris, A. M.; Watzky, M. A.; Finke, R. G. *Biochim. Biophys. Acta, Proteins Proteomics* **2009**, *1794*, 375.

(31) Finney, E. E.; Finke, R. G. *Chem. Mater.* **2009**, *21*, 4692.

(32) Galanakis, I.; Papanikolaou, N.; Dederichs, O. N. *Surf. Sci.* **2002**, *511*, 1−12.

(33) (a) Van Hardeveld, R.; Hartog, F. *Adv. Catal.* **1972**, *22*, 75−113. (b) Che, M.; Bennett, C. O. *Adv. Catal.* **1989**, *36*, 55−172.

(34) Watzky, M. A.; Finney, E. E.; Finke, R. G. *J. Am. Chem. Soc.* **2009**, *130*, 11959.

(35) (a) Bartholomew, C. H.; Farrauto, R. J. Catalyst Deactivation: Causes, Mechanisms, and Treatments. *Fundamentals of Industrial Catalytic Processes*, 2nd ed.; John Wiley & Sons: Hoboken, NJ, 2006; 260−336. (b) Datye, A. K.; Xu, Q.; Kharas, K. C.; McCarty, J. M. *Catal. Today* **2006**, *111*, 59. (c) Bartholomew, C. H. *Appl. Catal. A: Gen.* **2001**, *212*, 17.

(36) Ott, L. S.; Finke, R. G. *Chem. Mater.* **2008**, *20*, 2592−2601.

(37) Graham, C. R.; Finke, R. G. *Inorg. Chem.* **2008**, *47*, 3679.

(38) Hornstein, B. J.; Finke, R. G. *Inorg. Chem.* **2002**, *41*, 2720.

(39) Weiner, H.; Trovarelli, A.; Finke, R. G. *J. Mol. Catal. A* **2003**, *191*, 217.

(40) (a) Boehm, H.-P.; Knözinger, H. Nature and Estimation of Functional Groups on Solid Surfaces, in *Catalyst Science and Technology*; Anderson, J. R.; Boudart, M., Eds.; Springer: Berlin, 1983; p 39. (b) Sterrer, M.; Freund, H.-J. *Catal. Lett.* **2013**, *143*, 375−385.

(41) (a) Lin, Y.; Finke, R. G. *J. Am. Chem. Soc.* **1994**, *116*, 8335. (b) Lin, Y.; Finke, R. G. *Inorg. Chem.* **1994**, *33*, 4891.

(42) Widegren, J. A.; Aiken, J. D., III; Ozkar, S.; Finke, R. G. *Chem. Mater.* **2001** *13*, 312.

(43) Some useful references include: (a) Sachtler, W. M. H. Ensemble and Ligand Effects in Metal Catalysis, in *Handbook of Heterogeneous Catalysis*; Ertl, G.; Knozinger, H.; Weitkamp, J., Eds.; VCH: Weinheim, 1997; p 365. (b) van den Broek, A. C. M.; van Grondelle, J.; van Santen, R. A. *J. Catal.* **1997**, *167*, 417. (c) Jacobs, P. A.; Uytterhoeven, J. B.; Beyer, H. K. *J. Chem. Soc. Faraday Trans.* **1979**, *75*, 56.

(44) See http://members.dca.net/leipold/mk/advert.html for more information.

(45) "Finding a global extremum is, in general, a very difficult problem." Press, W. H.; Teukolsky, S. A.; Vetterling, W. T.; Flannery, B. P. Chapter 10. Minimization or Maximixation of Functions, in *Numerical Recipes in Fortran: The Art of Scientific Computing*, 2nd ed.; Cambridge University Press: Cambridge, 1992; p 387.

(46) Hoops, S.; Sahle, S.; Gauges, R.; Lee, C.; Pahle, J.; Simus, N.; Singhal, M.; Xu, L.; Mendes, P.; Kummer, U. *Bioinformatics* **2006**, *22*, 3067.